[30] ———, "Cycloid circulation of spiral waves in an excitable medium," *Biophysics* 31 (1986), 940–944.

[31] ———, *Simulation of wave processes in excitable media*, Manchester Univ. Press, Manchester UK, 1987.

[14] R. N. Miller & J. Rinzel, "The dependence of impulwse propagation speed on firing frequency, dispersion, for the Hodgkin-Huxley model," *Biophys. J.* 34 (1981), 227–259.

[15] G. K. Moe, W. C. Rheinboldt & J. A. Abildskov, "A computer model of atrial fibrillation," *Am. Heart J.* 67 (1964), 200–220.

[16] A. V. Panfilov & A. N. Rudenko, "Two regimes of scroll ring drift in three-dimensional active media," *Phys. D* 28 (1987), 215–218.

[17] A. V. Panfilov, A. N. Rudenko & V. I. Krinskii, "Vortical rings in three-dimensional active media with diffusion over two components," *Biophysics* 31 (1986), 926–931.

[18] A. M. Pertsov, E. A. Ermakova & A. V. Panfilov, "Rotating spiral waves in a modified Fitz-Hugh-Nagumo model," *Phys. D* 14 (1984), 117–124.

[19] R. D. Richtmyer & K. W. Morton, *Difference methods for initial-value problems*, Interscience Publishers, New York, 1967.

[20] L. S. Schulman & P. E. Seiden, "Percolation and galaxies," *Science* 233 (1986), 425–431.

[21] O. Selfridge, "Studies on flutter and fibrillation V. Some notes on the theory of flutter," *Arch. Inst. Cardiol. de Mexico* 18 (1948), 177–187.

[22] J. M. Smith & R. J. Cohen, "Simple finite-element model accounts for wide range of cardiac dysrhythmias," *Proc. Natl. Acad. Sci. USA* 81 (1984), 233–237.

[23] J. J. Tyson & J. P. Keener, "Singular perturbation theory of traveling waves in excitable media (A review)," *Phys. D* 32 (1988), 327–361.

[24] N. Wiener & A. Rosenblueth, "The mathematical formulation of the problem of conduction of impulses in a network of connected excitable elements, specifically in cardiac muscle," *Arch. Inst. Cardiol. de Mexico* 16 (1946), 205–265.

[25] A. T. Winfree, "Spiral waves of chemical activity," *Science* 175 (1972), 634–636.

[26] ———, *When time breaks down*, Princeton University Press, Princeton, NJ, 1987.

[27] A. M. Zhabotinskii & A. N. Zaikin, "Concentration wave propagation in two-dimensional liquid-phase self-oscillating system," *Nature* 225 (1970), 535–537.

[28] V. S. Zykov, "Analytical evaluation of the dependence of the speed of an excitation wave in a two-dimensional excitable medium on the curvature of its front," *Biophysics* 25 (1980), 906–911.

[29] ———, "Kinematics of the steady circulation in an excitable medium," *Biophysics* 25 (1980), 329–333.

References

[1] I. S. Balakhovskii, "Several Modes of excitation movement in ideal excitable tissue," *Biophysics* 10 (1965), 1175–1179.

[2] J. D. Dockery, J. P. Keener & J. J. Tyson, "Dispersion of traveling waves in the Belousov-Zhabotinskii reaction," *Phys. D* 30 (1988), 177–191.

[3] V. G. Fast & I. G. Efimov, "Stability of vortex rotation in excitable cellular medium," *Phys. D*, (submitted).

[4] M. Gerhardt, H. Schuster & J. J. Tyson, "A cellular automaton model of excitable media including curvature and dispersion II. Curvature, dispersion, rotating waves and meandering waves," *Phys. D* 46 (1990), 392–415.

[5] ———, "A cellular automaton model of excitable media including curvature and dispersion III. Fitting the Belousov-Zhabotinskii reaction," *Phys. D* 46 (1990), 416–425.

[6] ———, "A cellular automaton model of excitable media including curvature and dispersion," *Science* 247 (1990), 1563–1566.

[7] A. L. Hodgkin & A. F. Huxley, "A quantitative description of membrane current and its application to conduction and excitation in nerve," *J. Physiol.* 117 (1952), 500–544.

[8] W. Jahnke, W. E. Skaggs & A. T. Winfree, "Chemical vortex dynamics in the Belousov-Zhabotinskii reaction and in the two-variable Oregonator model," *J. of Physical Chem.* 93 (1989), 740–749.

[9] W. Jahnke & A. T. Winfree, "A survey of spiral wave behaviors in the Oregonator model," *Intern. J. of Chaos and Bifurcations* (submitted).

[10] J. P. Keener, "A geometrical theory for spiral waves in excitable media," *SIAM J. Appl. Math.* 46 (1986), 1039–1056.

[11] S. A. MacKay, "Computer Simulation of aggregation in Dictyostelium discoideum," *J. Cell Sci.* 33 (1978), 1–16.

[12] M. Markus, "Dynamics of a cellular automaton with randomly distributed elements," in *Mathematical Population Dynamics: Proc. Second Intern. Conf.*, Marcel Dekker, New York, NY, (in press).

[13] M. Markus & B. Hess, "Isotropic cellular automaton for modeling excitable media," *Nature* 347 (Sept. 1990), 56–58.

8. Conclusion

We show how to calculate the effective diffusion coefficient of several different masks that are used in cellular automata simulations of excitable media. Experimental investigation shows that the linear curvature relationship $N = c - D\,K$ holds reasonably well for most masks and thresholds considered. However, we find that the apparent diffusion coefficient (D) is not independent of the threshold, as it should ideally be. The best masks in this respect are the combinations of square and diamond masks, for which the apparent diffusion coefficient varies little with threshold and is (when averaged over all thresholds) very close to the effective diffusion coefficient predicted by theoretical considerations. These masks are also computationally efficient. Therefore these masks are considered the best candidates for the development of cellular automata that mimic the reaction-diffusion equations of excitable media.

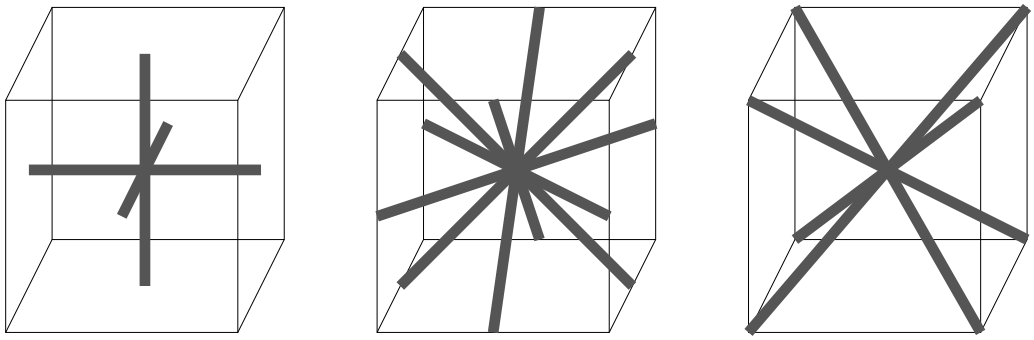

Figure 16: *Scan directions for the three different possibilities for three-dimensional masks.*

Figures 14 and 15 show that the variance is considerably smaller for the combination mask than for the simple square mask.

7. Possible extensions of masks into three dimensions

For three-dimensional simulations, the only change necessary for our automaton is to define a three-dimensional mask. For the square mask, the obvious extension is the cubic mask, a convolution of strips in the x-, y-, and z-directions. For the diamond mask, extensions are not so obvious, because in the three-dimensional case there are many more symmetries than in the two-dimensional case.

Two possibilities exist for convolutions of strips that are fully symmetric:

- Apply a diamond mask in each of the three planes, i.e., in the xy-plane, in the yz-plane, and in the xz-plane. This amounts to a total of six strip operations and is completely symmetrical.
- Do one strip in each of the four space diagonals of a cube. This amounts to four strip operations and is also fully symmetric.

Both possibilities of diagonal masks suffer from the same problem of the diamond mask in two dimensions: there are holes left in the mask. Therefore, both masks need to be combined with a cubic mask to eliminate these holes, the same way this is done in two dimensions. Figure 16 shows the three possibilities for symmetric masks by indicating the scan directions in a cube.

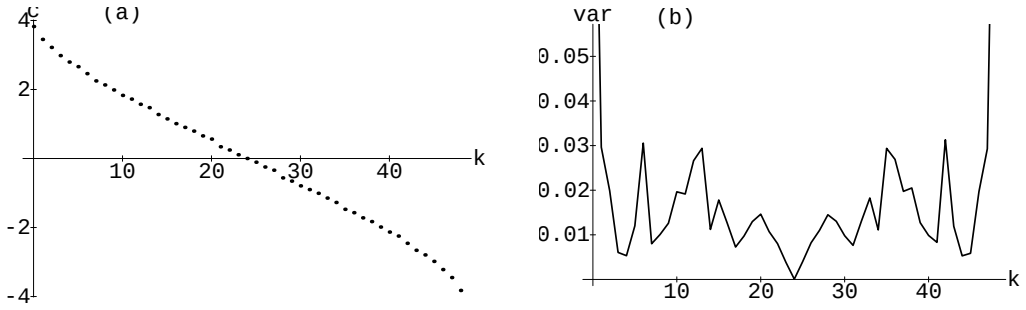

Figure 14: *Average speed (a) and variance of speed (b) for planar waves as a function of threshold for the square mask of radius 3.*

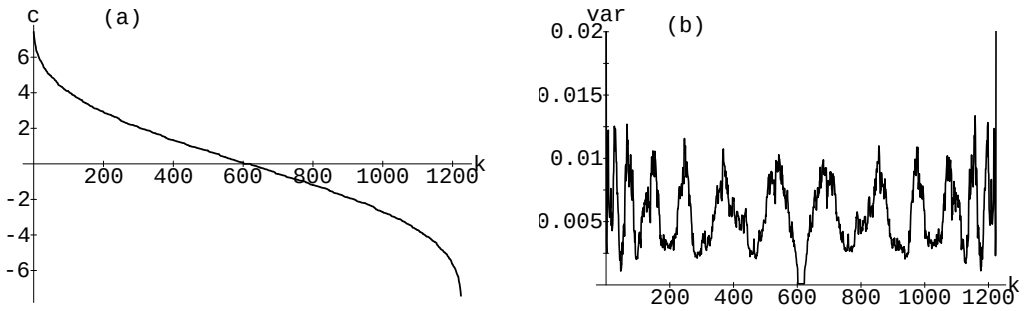

Figure 15: *Average speed (a) and variance (b) for planar waves as a function of threshold for the combination mask diamond(2)*square(3).*

In a series of experiments, the propagation speed of plane waves is measured. Two examples of how the speed depends upon the angle of a wave are given in Figure 13. Both examples use the combination mask diamond(2)*square(3), at thresholds 246 and 294. It can be seen that in both cases the speed in the horizontal direction is 2. The speed in the diagonal direction is $2.828 = 4/\sqrt{2}$ and $2.121 = 3/\sqrt{2}$. For intermediate angles the speed is relatively constant even in (a). One way to assess the isotropy of wave propagation is to calculate the average planar wave speed over all angles and the variance about this average. Figures 14 and 15 show the results for some masks. It can be seen that the average speed is a monotonously decreasing function of the threshold (which is almost identical to the speed function derived from circular waves). The variance of the speed is very different for different thresholds.

If isotropic behavior is very important, it might be useful to restrict the possible thresholds to those with small variance of the speeds. This reduces the number of available speeds, however.

Table 3: *Multiples of 1 and $1/\sqrt{2}$ (corresponding to possible speeds of planar waves in horizontal and diagonal directions).*

horizontal	*diagonal*
0	*0*
	0.707
1	*1.414*
2	*2.121*
3	*2.828*
4	*3.536*
	4.243
5	*4.950*
6	*5.657*
	6.364
7	*7.071*
8	*8.485*
9	*9.192*
10	*9.899*

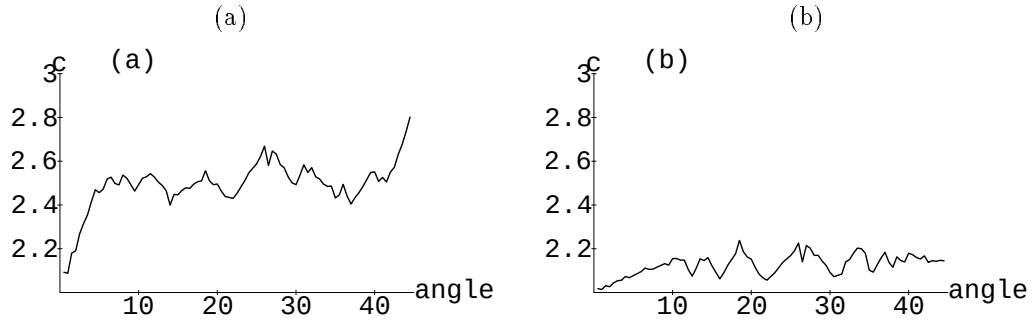

Figure 13: *Speed of planar waves as a function of the angle for threshold 246 (a) and 294 (b).*

12. Here a square mask of radius 1 with threshold 0 (i.e., a cell becomes excited if > 0 neighbors are excited) gives rise to waves with speed 1 in the horizontal (vertical) direction and speed $\sqrt{2}$ in the diagonal directions. For thresholds 1 and 2, the horizontal speed is still 1, whereas the diagonal speed is $1/\sqrt{2}$. For thresholds 3,4 and 5, both speeds are 0.

In general, the speed of a plane wave in the horizontal direction can only assume integer values. The speed in the diagonal direction can only assume multiples of $1/\sqrt{2}$. Table 3 shows these values. It can be seen that there are certain wave speeds for which horizontal and diagonal speed can be very close together (e.g., 5) and others for which the difference is much bigger (e.g., 6). Similar arguments can be made for waves traveling with slopes $\frac{p}{q}$, where p and q are small integers.

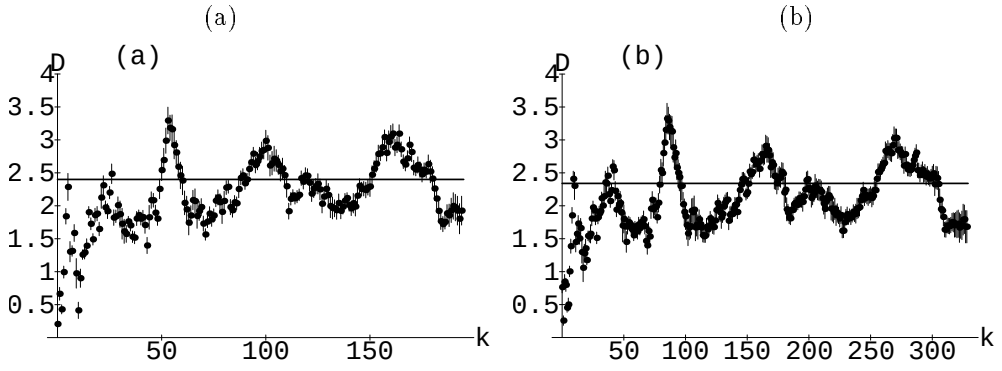

Figure 11: *Diffusion coefficient vs. threshold for Gaussian masks with* $C = 11, d = 3.5$ *(a) and* $C = 20, d = 3$ *(b) . The linear fit used 62 curvatures between* -0.1 *and* $+0.1$ *in steps of 0.003* ($\delta = \frac{1}{3}$).

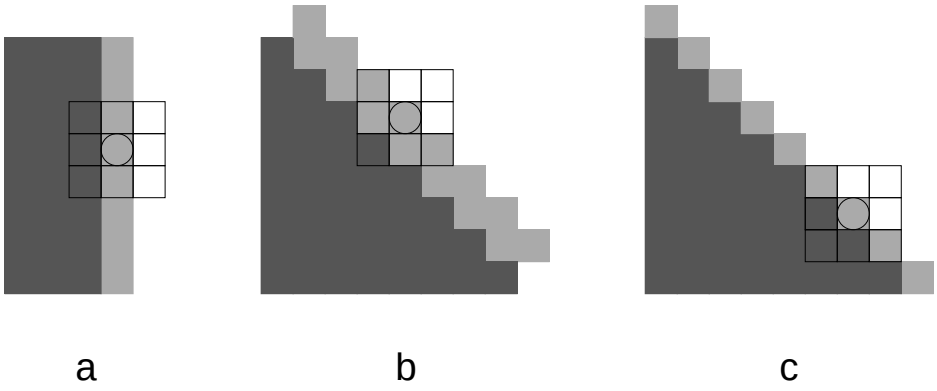

Figure 12: *Speed of planar waves in different directions. Dark grey is wave before updating, light grey after updating. (a) is a horizontal wave, (b) and (c) are diagonal waves with thresholds 0 for (b) and 1 or 2 for (c).*

6. Dependence of plane wave speed on propagation direction

One basic parameter in the design of a cellular automaton is the choice of the grid or lattice. Most researchers using cellular automata for excitable media choose a square lattice because it is easier to work with numerically.

For a given mask and a given threshold, the speed of a plane wave depends upon the direction of the wave in relation to the grid. A simple example with a small mask illustrates this in Figure

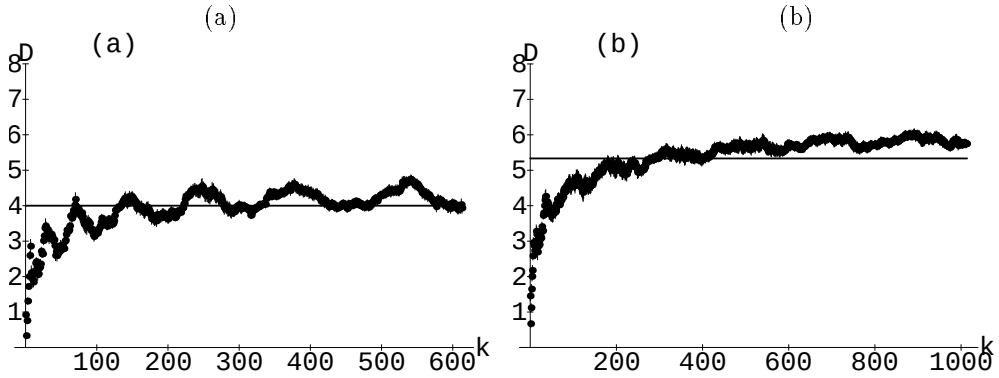

Figure 9: *Diffusion coefficient vs. threshold for combination masks (a) diamond(2)∗ square(3) and (b) diamond(2)∗square(4).*

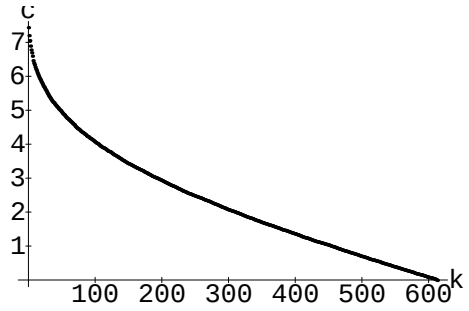

Figure 10: *Speed vs. threshold for combination mask diamond(2)∗square(3).*

5.6. Gaussian mask.

The Gaussian mask gives unexpectedly bad results in this experiment. The diffusion coefficient jumps in a very broad range and the average is not very close to the theoretical value. Some examples are shown in Figure 11 and some averaged results are shown in the table, where $\mathcal{D}_m$ is the diffusion coefficient calculated from the actual mask (see also Table 1 and remarks in Section 3). Note that the Gaussian mask can only be tested for small $\mathcal{D}_m$, because the computation gets too expensive for larger masks.

parameters C,d	D_{av}	$\mathcal{D}_m$
11, 3.5	2.16	2.40
20, 2	1.26	1.53
40, 3	2.32	2.54
20, 3	2.10	2.34
10, 2.5	1.39	1.65

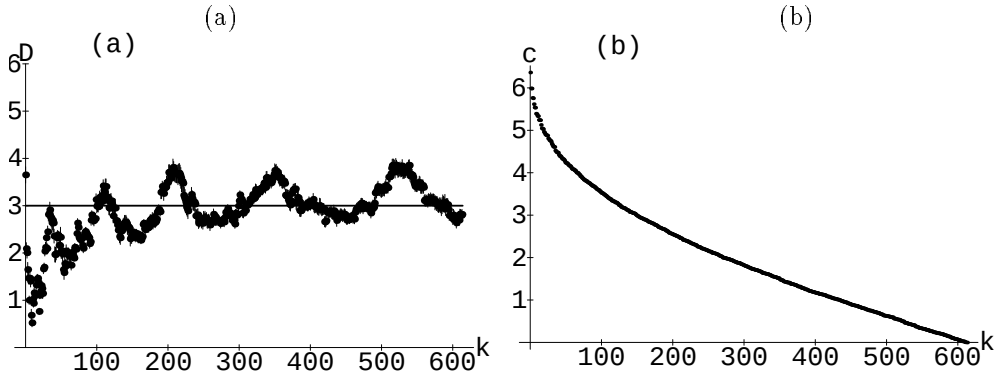

Figure 8: *(a) Diffusion coefficient vs. threshold and (b) speed vs. threshold for convolution mask square(2)∗square(3).*

radii	D_{av}	$\mathcal{D}_m$
2,2	1.85	2
2,3	2.89	3

5.5. Combination diamond-square

The convolution of a diamond mask with a square mask seems to be the best mask of those under consideration here. The curve of D vs. k is fairly flat and smooth for this mask. Also, the averaged D is very close to the theoretical prediction. Figures 9 and 10 show the results for two such masks. We take into consideration only those combinations of radii where the radius of the diamond mask is not greater than the radius of the square mask. The other combinations have masks for which the weights are not monotonously decreasing from the inside to the outside. Experiment and theory compare as follows:

radii	D_{av}	$\mathcal{D}_m$
1, 2	1.49	1.66
2, 2	2.87	3
1, 3	2.52	2.66
2, 3	3.93	4
3, 3	6.10	6
2, 4	5.37	5.33

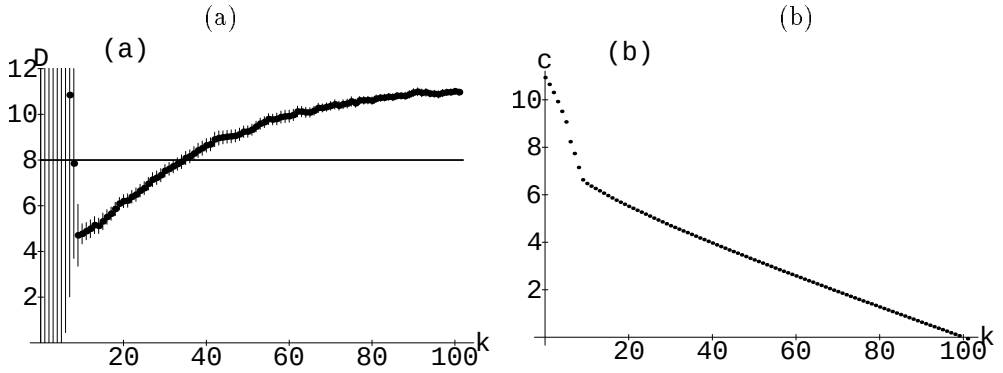

Figure 6: *(a) Diffusion coefficient vs. threshold and (b) speed vs. threshold for random circle mask of radius 8. The linear fit used 94 curvatures between* -0.1 *and* $+0.1$ *in steps of 0.002* ($\delta = \frac{1}{3}$). *The horizontal line marks* $D = \mathcal{D}_m$.

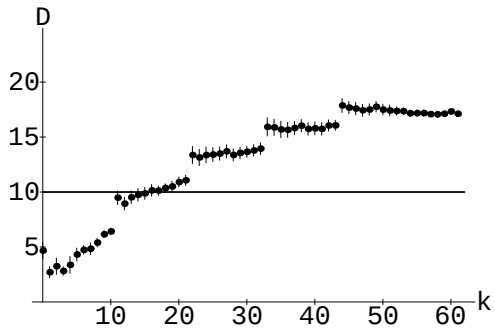

Figure 7: *Diffusion coefficient vs. threshold for diamond mask of radius 5. Same conditions as in Figure 6.*

radius	D_{av}	$\mathcal{D}_m$
4	8.43	6.66
5	12.83	10
6	17.89	14

5.4. Combination square-square

The convolution of two square masks shows a new effect: the curve of D vs. k is not monotone any more, but fluctuates up and down. On the other hand, the average over all thresholds is close to the theoretically predicted value. Figure 8 shows the result from the convolution of a radius 2 square mask with a radius 3 square mask. The averaged result is:

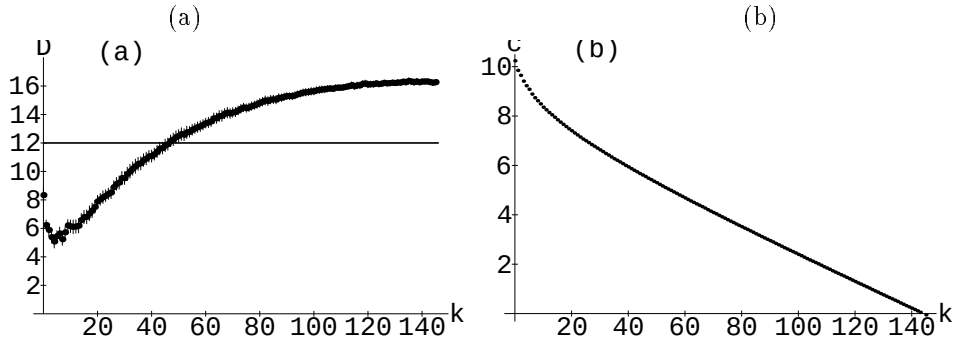

Figure 5: *(a) Diffusion coefficient vs. threshold and (b) speed vs. threshold for square mask of radius 8. The linear fit used 87 curvatures between* -0.1 *and* $+0.1$ *in steps of 0.002* ($\delta = \frac{1}{3}$). *The horizontal line marks* $D = \mathcal{D}_m$.

5.2. Random circle mask

The random circle mask exhibits very strong irregularities for small thresholds. Here there is no linear relationship between N and curvature K, so that the error in the linear fit is very large. Beyond some point, the curve for this mask looks almost exactly like that for a square mask of slightly smaller radius. This is not surprising, since the center part of a circle looks similar to the center part of a square. The close similarity comes from the fact that in both cases the weight of all cells is 1. The random mask is not a good choice if the aim is to achieve a threshold-independent D. Figure 6 shows the D plots and the speed plots for radius 8. The value D_{av} compares as follows to the theoretical value:

radius	D_{av} averaged over all k	Average over all but first 8	$\mathcal{D}_m$
6	6.63	5.01	4.5
8	9.73	8.99	8

5.3. Diamond mask

Similar to the square mask is the diamond mask, with additional jumps, which are probably caused by the holes in the mask. Figure 7 shows the results for the diamond mask with radius 5. The results of the averaging are:

and negative curvatures. (The negative curvature experiments start with the exterior of the circle excited.)

From the graphs we see that using the range of curvatures from -0.1 to 0.1 seems to be the most suitable for determining the diffusion coefficient, since here the graphs are smoother and the errors are smaller than for other curvature ranges.

Using this range and six different centers with $\delta = 1/3$, many different masks are tested. Although most masks have a fairly flat D-curve for high thresholds and exhibit a linear curvature relationship for almost all thresholds (most error bars are fairly small), the result shows that *most masks do not have a constant slope D over all thresholds k*. For all masks, very small thresholds result in a slope that is much too small. In order to be able to compare experiment and theoretical prediction, the average of D for all thresholds k is calculated as D_{av}.

5. Diffusion coefficients for different masks

5.1. Square mask

For square masks the slope D is *not* independent of threshold; rather, $D(k)$ is clearly an increasing function. Figure 5 shows the function $D(k)$ for radius 8, as well as the speed curve, $c(k)$, for this mask. Although D increases with k, the average value of D over all thresholds is not far from the expected value ($\mathcal{D}_m$):

radius	D_{av}	$\mathcal{D}_m$
4	3.23	3.33
6	7.14	7
7	9.77	9.33
8	12.94	12
9	16.71	15

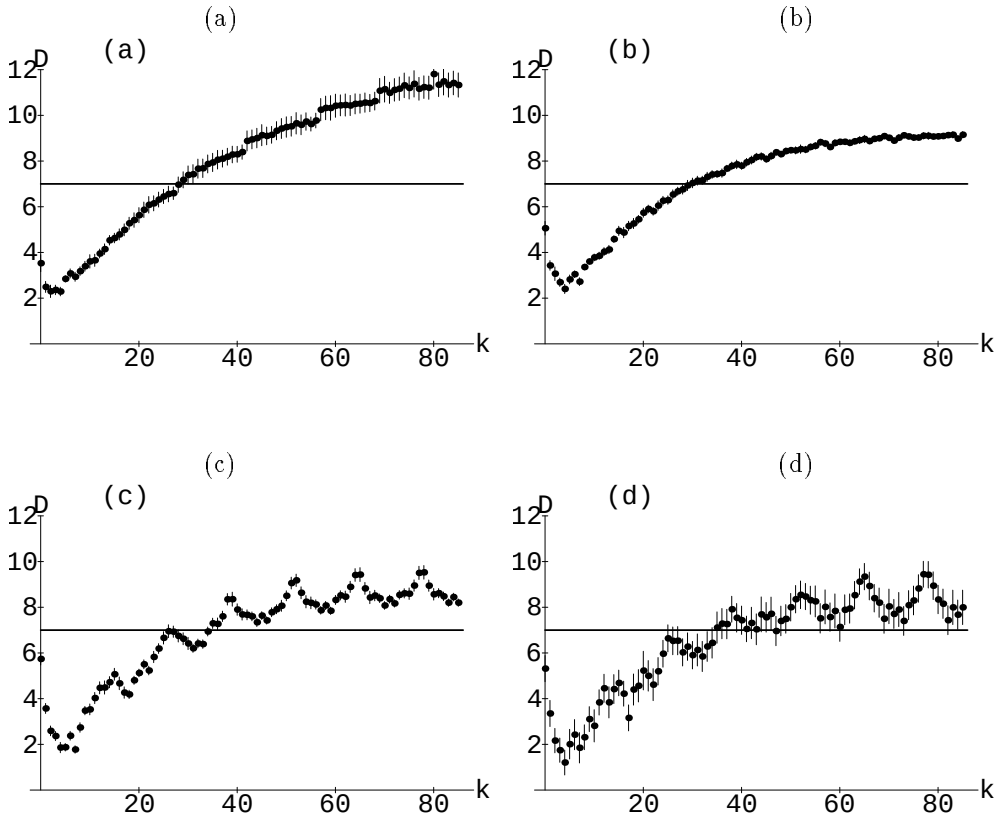

Figure 4: *Diffusion coefficient vs. threshold for square mask radius 6 for different curvature ranges. Error bars indicate 99% confidence interval and the horizontal line marks $D = \mathcal{D}_m$. (a) Curvature -0.2 .. +0.2, increment 0.01. (b) Curvature -0.1 .. +0.1, increment 0.005. (c) Curvature -0.05 .. +0.05, increment 0.002. (d) Curvature -0.025 .. +0.025, increment 0.0008.*

Two important points should be mentioned: large curvatures (small radii) are limited by the fact that the number of 1's in the initial circle needs to be big enough to exceed the threshold of the mask. Otherwise it is not possible to calculate a speed. The other limitation is for small curvatures (large radii). Since the size of the array used for these simulations is 150×150, radii above $(150 - 3 \cdot \text{masksize})$ are not possible, because the resulting circle would exceed the simulation domain. Therefore, curvatures between -0.01 and 0.01 are not possible. The range of curvatures used should be at least $-0.03 \cdots 0.03$, so that the measured points form a line for both positive

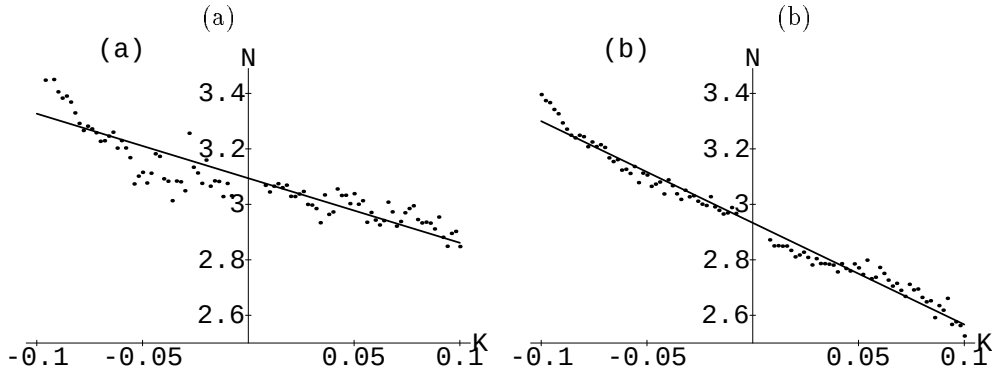

Figure 3: *Two examples of normal speed N as a function of curvature K: (a) for random circle(5) with threshold 10 and (b) for diamond(2)∗square(3) with threshold 200.*

be linear for all thresholds, and that the slope of the line (D) be independent of threshold. For the simulations, the units of space and time are $\Delta t = 1$ and $h = 1$. These are the units that N, c, K, and therefore also D are measured in. Therefore from (9), we expect that D should be close to $\mathcal{D}_m$, the theoretical diffusion coefficient of the mask.

The experiment is repeated for each mask for each threshold. To illustrate the resulting dependence of speed on curvature, Figure 3 shows exemplary plots of speed vs. curvature. Fig 3(a) is from the random circle mask with radius 5, using 94 different curvatures from -0.1 to 0.1, where $\delta = 0.34$ and the threshold $k = 10$. Fig. 3(b) is for a convolution of a square mask with radius 3 and a diamond mask with radius 2. The threshold here is $k = 200$, all other parameters are the same. For both examples it is obvious that a linear fit is a good approximation to describe the data sets. In (a) one would get $N \approx 3.09 - 2.33K$, where the 99% confidence interval for the slope is 2.33 ± 0.28. The corresponding values for (b) are $N \approx 2.93 - 3.67K$ where the confidence interval for D is 3.67 ± 0.13.

The first question to be solved is the range of curvatures that should be used. In a small series of experiments, different ranges of curvatures are used to calculate a linear fit to the obtained normal velocities (as a function of curvature). Also, a confidence interval for the slope of the obtained fit is calculated. The results are presented in Figure 4 for a square mask of radius 6.

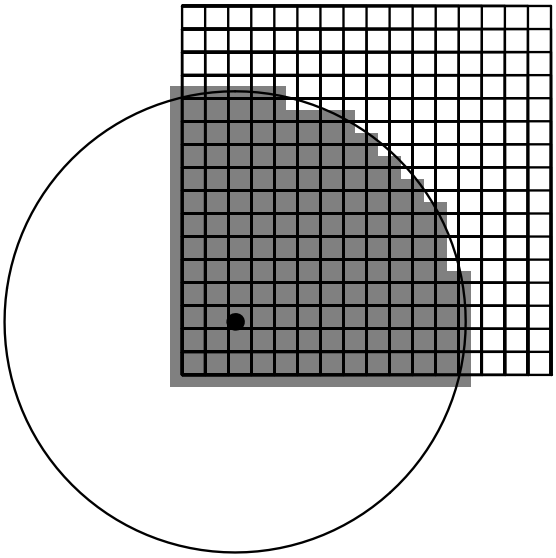

Figure 2: *Circle of 1-cells with radius 10.*

An average normal velocity is determined by calculating the average distance to the center $(0, 0)$ of all cells that lie on the border of the resulting region of 1's. Specifically, the average of all cells that are either 1 and have immediate neighbors which are 0 or that are 0 and have immediate neighbors that are 1, is taken. (Immediate neighbor here means that exactly one coordinate differs by exactly one.) From the resulting value the radius of the original circle is subtracted. This is the speed a wavefront with curvature K would have if the threshold were k in the region of the wavefront.

It is important to recognize the discreteness of the underlying grid. Small radii lead to regions of 1's on the grid that look far from circular. To reduce this effect, the experiment is repeated many times with different origins of the circle with respect to the origin of the grid. The setup used here is to take all positions of the origin in $(x, y) \in \{0, \delta, 2\delta, 3\delta, \cdots, 1-\delta\} \times \{0, \delta, 2\delta, 3\delta, \cdots, 1-\delta\}$. Mostly, δ is chosen to be $1/3$ or $1/4$. Symmetry considerations lead to the elimination of the cases where $y < x$, so that $(1/\delta) \cdot (1/\delta + 1)/2$ positions of the origin are simulated and the results averaged. The result is the speed that is reported for the given initial radius r and threshold k.

To determine the relationship $N = c - D\,K$, this experiment is repeated for many different curvatures of the initial circle. As was stated earlier, it is desirable that the N vs. K relationship

4. Wave propagation and curvature effects

Several researchers are using comparable cellular automata models to simulate excitable media [3,4,5,6,13]. All these models have two features in common: 1. They all have a resting and an excited state. 2. The transition from resting to excited state occurs when the number of excited cells in some neighborhood exceeds a threshold k. The neighborhoods and the threshold vary from model to model.

In this section, we seek to verify numerically the curvature relationship $N = c - D\,K$, where N is the normal velocity of the wave front, c is the speed of a planar wavefront, D is the diffusion coefficient of the excitation variable and K is the curvature of the wavefront. To simulate excitable media reliably, it is desirable that this relationship be linear in K and that D be independent of the threshold k of the cellular automaton.

In order to investigate the validity of the curvature relationship, the following simple experiment is set up:

On a grid of size 150×150, all cells are set to 0 except for a circular area, which is initialized to 1. Since there is an inherent symmetry in the masks used here, only one quarter circle is used, where the center of the circle is near coordinates $(0, 0)$. Mirror boundary conditions complete the circle according to the size of the mask. The circular area has a radius r, which is equivalent to having curvature $K = \frac{1}{r}$. This situation is depicted in Figure 2, where the center of the circle is at $(0.3, 0.3)$, the boundary is 2 cells wide (for use with a mask of radius 2) and the circle has radius 10. Grey squares indicate the cells (centered at the mesh points) that are 1. The criterion is that the mesh point (intersection of vertical and horizontal lines) must be inside the circle or on the circle.

Now the mask under consideration is applied to this array, giving a count of the number of excited (value = 1) neighbors for each cell. Then a thresholding function is applied, which replaces a cell's value by 1 if the neighborhood count S is greater than the specified threshold k. Otherwise the cell value becomes 0. This procedure mimics the spread of excitation in cellular automaton models of excitable media.

Table 1: *Diffusion coefficients for Gaussian masks.*

C	d	$\mathcal{D}_m$
11	3.5	2.399
21.5	5.1	4.072
10	5	3.460
100	5	4.617
1000	5	4.924
10000	5	4.988
100000	5	4.998

Table 2: *Diffusion coefficients $\mathcal{D}_m$ for commonly used masks.*

radius	square	diamond	random circle (from (13))
1	0.33	0.66	0.125
2	1	2	0.5
3	2	4	1.125
4	3.33	6.66	2
5	5	10	3.125
6	7	14	4.5
7	9.33	18.66	6.126
8	12	24	8

These functions are normalized so that

$$S = \int_{-\infty}^{\infty} \int_{-\infty}^{\infty} a(m,n)\, dm\, dn = 1.$$

The result of carrying out the integration for the square mask is

$$\mathcal{D}_m \approx \frac{(2\,r+1)^2}{24} = \frac{r(r+1)}{6} + \frac{1}{24},$$

for the random circle mask

$$\mathcal{D}_m \approx \frac{r^2}{8},$$

and for the Gaussian mask

$$\mathcal{D}_m \approx d.$$

For the Gaussian mask, this approximation is good only if C is sufficiently large. In Table 1 several different parameter combinations for the Gaussian mask are listed, together with the value $\mathcal{D}_m$ one obtains from carrying out the summation in (7) explicitly.

The value $\mathcal{D}_m$ is important for further simulations, therefore it is listed for several masks in Table 2.

The fifth type of mask we consider is the random circle mask, proposed and used by Markus and Hess [13].

In order to use these masks, it is necessary to find the mask diffusion coefficient $\mathcal{D}$, denoted by $\mathcal{D}_m$ in the sequel. It can be easily calculated from (7) for any given mask. For some mask types it is possible to determine a general formula that gives the value $\mathcal{D}_m$ as a function of the parameters (e.g., radius) of the mask. For the square mask we get

$$\mathcal{D}_m = \frac{r\,(r+1)}{6}$$

and for the diamond mask

$$\mathcal{D}_m = \frac{r\,(r+1)}{3}.$$

For the convolutions of square and diamond masks, $\mathcal{D}_m$ can be calculated from the sum rule $\mathcal{D}_{m3} = \mathcal{D}_{m1} + \mathcal{D}_{m2}$.

For the Gaussian and random circle masks, $\mathcal{D}_m$ cannot be calculated easily in closed form, but it is easy to obtain integral approximations to $\mathcal{D}_m$. In general, $\mathcal{D}_m$ can be approximated as

$$\mathcal{D}_m \approx \int_0^\infty \int_0^\infty a(m,n)\left(m^2+n^2\right)\,dm\,dn. \tag{13}$$

The functions $a(m,n)$ for the different masks are

$$\text{square mask:} \qquad a(m,n) = \begin{cases} \dfrac{1}{(2\,r+1)^2}, & \text{if } |m| \le r+\frac{1}{2} \text{ and } |n| \le r+\frac{1}{2}, \\ 0, & \text{otherwise;} \end{cases}$$

$$\text{circle mask:} \qquad a(m,n) = \begin{cases} \dfrac{1}{\pi\,r^2}, & \text{if } m^2+n^2 \le r^2, \\ 0, & \text{otherwise;} \end{cases}$$

$$\text{Gaussian mask:} \qquad a(m,n) = \frac{1}{2\sqrt{\pi\,d}}\; e^{-\frac{m^2+n^2}{4d}}.$$

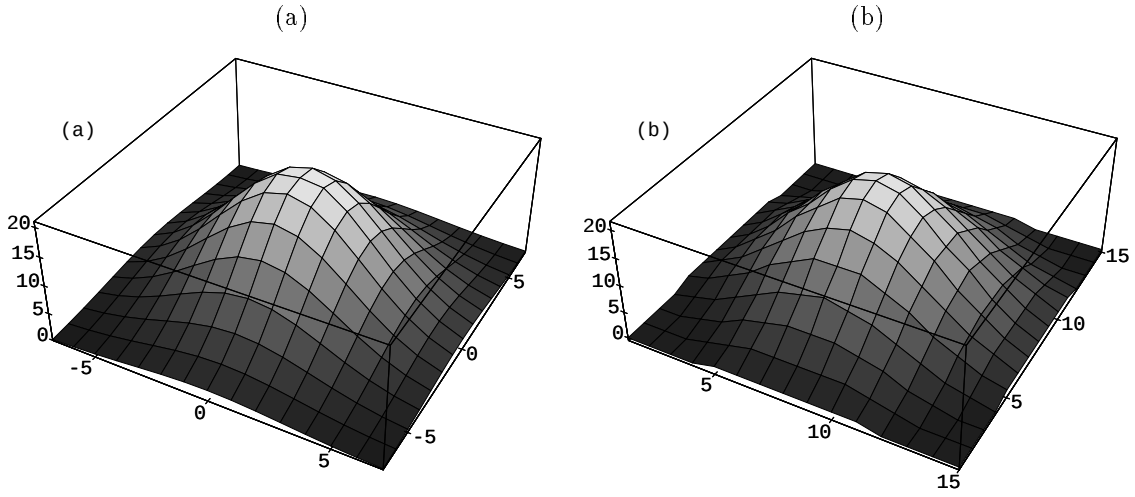

Figure 1: *Comparison of (a) Gaussian mask without truncation to integers and (b) combination mask diamond(2)∗square(3).*

a mask in a time independent of its size. Instead the computational effort required is proportional to the number of elements in the mask. These masks are created using the formula

$$a_{m,n} = \left\lfloor C\ e^{\frac{-(m^2+n^2)}{4d}} \right\rfloor .$$

In [3] a mask was used that differs only slightly from the mask obtained with this formula and parameters $C = 11, d = 3.5$. The combination mask diamond(2)∗square(3), which we find very useful, can almost be obtained by this formula with parameters $C = 21.5$ and $d = 5.125$. The combination mask and the true Gaussian mask differ only in 16 out of 225 entries. None of the entries differs by more than one. In Figure 1, both masks are shown. Combination masks are similar to Gaussian masks because each time step can be thought of as two sub-steps using simpler (non-gaussian) masks. As we have just shown, these simpler masks, when iterated, model the diffusion operator, and consequently they smooth a unit pulse into a Gaussian distribution. Clearly, the alternation of diamond and square masks is quite effective at generating a nearly Gaussian distribution in only one compound step. The only purpose of the Gaussian masks in the current setting is to compare their performance with that of the other proposed masks which are computationally feasible.

The computation necessary to perform this neighborhood count operation is approximately double that necessary to compute the simple square mask, since it is applied two times. The time is also almost independent of the radii r_1 and r_2.

The same technique of scanning through the grid and keeping a running total can also be applied in directions other than horizontal and vertical. Our next mask is constructed by scanning in both diagonal directions. This results in a diamond shaped mask (but with holes inside):

$$\text{diamond}(1) = \begin{bmatrix} 0 & 0 & 1 & 0 & 0 \\ 0 & 1 & 0 & 1 & 0 \\ 1 & 0 & 1 & 0 & 1 \\ 0 & 1 & 0 & 1 & 0 \\ 0 & 0 & 1 & 0 & 0 \end{bmatrix}.$$

The computational complexity of this mask is almost independent of its size and it is about the same as that for the simple square mask.

Convolutions of diamond masks and square masks give masks that almost have a round shape. These diamond-square masks seem very useful. For example, the convolution of a square mask of radius 1 and a diamond mask of radius 1 yields

$$\text{diamond}(1)*\text{square}(1) = \begin{bmatrix} 0 & 0 & 1 & 1 & 1 & 0 & 0 \\ 0 & 1 & 2 & 3 & 2 & 1 & 0 \\ 1 & 2 & 4 & 4 & 4 & 2 & 1 \\ 1 & 3 & 4 & 5 & 4 & 3 & 1 \\ 1 & 2 & 4 & 4 & 4 & 2 & 1 \\ 0 & 1 & 2 & 3 & 2 & 1 & 0 \\ 0 & 0 & 1 & 1 & 1 & 0 & 0 \end{bmatrix}.$$

All masks used here are constructed to model diffusion processes in one way or another. The effect of diffusion on a unit pulse can be described as

$$\frac{1}{2\sqrt{\pi D t}}\, e^{\frac{-r^2}{4D\,t}},$$

where D is a diffusion coefficient. This suggests using a mask whose elements drop off in magnitude like a Gaussian function of distance from the origin. It is not possible to compute the effect of such

3. Neighborhood operators used

Since we are looking at large neighborhoods, the application of the neighborhood operators needs to be very fast even for large neighborhoods. There are some neighborhoods that have the property that the computation time required is essentially independent of the neighborhood size. The simplest of these operators is the square mask:

$$\text{square}(1) = \begin{bmatrix} 1 & 1 & 1 \\ 1 & 1 & 1 \\ 1 & 1 & 1 \end{bmatrix}$$

(here radius 1), which is constructed as the convolution of

$$\begin{bmatrix} 1 \\ 1 \\ 1 \end{bmatrix} \text{ and } \begin{bmatrix} 1 & 1 & 1 \end{bmatrix}.$$

In general, a square mask of radius r has size $(2r+1)^2$ and can be generated by the convolution of row and column vectors of length $2r+1$. Each of these operators can be implemented as a column-wise (respectively row-wise) scan through the grid where a running count is kept, and, in going from one cell to the next, one cell at the top (right) is added and one cell at the bottom (left) subtracted from the current count. In this way the effect of a square mask of radius r can be calculated by just four additions per grid point, independent of the size of the mask. Square masks were favored by Gerhardt, Schuster and Tyson [4,5,6].

Another mask can be constructed by applying the square mask to the neighborhood count which resulted from another square mask. In other words, this new mask is a convolution of two square masks with radii r_1 and r_2. For $r_1 = 1$ and $r_2 = 1$ this results in the mask

$$\text{square}(1)*\text{square}(1) = \begin{bmatrix} 1 & 2 & 3 & 2 & 1 \\ 2 & 4 & 6 & 4 & 2 \\ 3 & 6 & 9 & 6 & 3 \\ 2 & 4 & 6 & 4 & 2 \\ 1 & 2 & 3 & 2 & 1 \end{bmatrix}.$$

New masks can be created as convolutions of smaller masks. Let mask a_3 be the convolution of masks a_1 and a_2. The effect of applying a_3 to u is

$$a_3 * u = (a_1 * a_2) * u = a_1 * (a_2 * u),$$

since convolution is an associative operator. Now according to (6), $(a_2 * u)$ is described as

$$\begin{aligned} u' &= (a_2 * u) \\ &= S_2\ u + h^2\ \mathcal{D}_2 \nabla^2 u + \frac{h^4}{12} E_2(u) + \mathcal{O}(h^6). \end{aligned} \tag{10}$$

The mask a_1 can also be described in terms of S_1 and $\mathcal{D}_1$:

$$\begin{aligned} u'' &= (a_1 * u') \\ &= S_1\ u' + h^2\ \mathcal{D}_1 \nabla^2 u' + \frac{h^4}{12} E_1(u') + \mathcal{O}(h^6). \end{aligned} \tag{11}$$

Then

$$\begin{aligned} u'' &= (a_1 * u') = a_1 * a_2 * u \\ &= S_1 \cdot S_2 \cdot u + S_1 \cdot h^2\ \mathcal{D}_2 \nabla^2 u + S_2 \cdot h^2\ \mathcal{D}_1 \nabla^2 u + \mathcal{O}(h^4) \\ &= S_1 \cdot S_2 \cdot u + h^2 \left(S_1 \cdot \mathcal{D}_2 + S_2 \cdot \mathcal{D}_1\right) \nabla^2 u + \mathcal{O}(h^4) \\ &= S_3 \cdot u + h^2\ \mathcal{D}_3 \nabla^2 u + \mathcal{O}(h^4)\ . \end{aligned} \tag{12}$$

Therefore $S_3 = S_1 \cdot S_2$ and $\mathcal{D}_3 = S_1 \cdot \mathcal{D}_2 + S_2 \cdot \mathcal{D}_1$.

The same result is obtained when the algebraic expressions for the convolution are inserted into the definitions of $\mathcal{D}$ and S (7). For our updating scheme (8), we have $S_1 = S_2 = 1$ and therefore $S_3 = 1$ and $\mathcal{D}_3 = \mathcal{D}_1 + \mathcal{D}_2$.

When used as finite difference methods, big masks have an error in the same order as the simple 5-point operator. The advantage of big masks is that they allow larger time steps, as it is obvious in (9) that a larger $\mathcal{D}$ (while D is fixed) leads to a larger Δt.

with

$$
\begin{aligned}
S &= a_{0,0} + 4 \sum_{m=0}^{r} \sum_{n=1}^{r} a_{m,n}\,, \\
\mathcal{D} &= \sum_{m=0}^{r} \sum_{n=1}^{r} \left(m^2 + n^2\right) a_{m,n}\,, \qquad \text{and} \\
E(u(t_k\,, x_i\,, y_j)) &= \sum_{m=0}^{r} \sum_{n=1}^{r} a_{m,n} \Big[\left(m^4 + n^4\right) \left(u^{(0,0,4)}(t_k\,, x_i\,, y_j) + u^{(0,4,0)}(t_k\,, x_i\,, y_j)\right) \\
&\qquad\qquad + 12 m^2 n^2 u^{(0,2,2)}(t_k\,, x_i\,, y_j) \Big],
\end{aligned}
\tag{7}
$$

where S and $\mathcal{D}$ are independent of $u(t, x, y)$. The characteristics of the finite difference scheme can be described in terms of S and $\mathcal{D}$, which are dependent only on the mask, and E to describe the error. S is the sum of all entries in the mask, and $\mathcal{D}$ is one-fourth of the weighted sum over all entries of the squared distances from the center of the mask.

Consider an updating scheme where the data at time $t + \Delta t$ is the result of the convolution of the data at time t and a mask:

$$
\begin{aligned}
u_{i,j}^{k+1} &= (a * u^k)_{i,j} \\
&= S \cdot u_{i,j}^k + h^2 \mathcal{D} \cdot \left(\nabla^2 u^k\right)_{i,j} + \mathcal{O}(h^4) \\
&\approx u_{i,j}^k + D\,\Delta t\, \left(\nabla^2 u^k\right)_{i,j}\,.
\end{aligned}
\tag{8}
$$

The last part is the demand from the differential equation for diffusion (1). It is immediately obvious that this requires $S = 1$ and

$$
D = \mathcal{D}\frac{h^2}{\Delta t} \iff D = \frac{h^2}{\Delta t} \sum_{m=0}^{r} \sum_{n=1}^{r} a_{m,n} \left(m^2 + n^2\right). \tag{9}
$$

An argument similar to the one in [19,page 12] can be used to show that this finite difference method is stable at least if $\forall i, j : a_{i,j} \geq 0$.

All masks considered here are assumed to have the following symmetry properties, where $a_{m,n}$ denotes the weight at position $[m,n]$ in the mask, which is centered around $[0,0]$:

$$\forall m,n \geq 0 : a_{m,n} = a_{-m,n} = a_{m,-n} = a_{-m,-n} = a_{n,m}. \tag{3}$$

For example, a mask of radius 2 has the general shape

$$a = \begin{bmatrix} a_{2,2} & a_{1,2} & a_{0,2} & a_{1,2} & a_{2,2} \\ a_{1,2} & a_{1,1} & a_{0,1} & a_{1,1} & a_{1,2} \\ a_{0,2} & a_{0,1} & a_{0,0} & a_{0,1} & a_{0,2} \\ a_{1,2} & a_{1,1} & a_{0,1} & a_{1,1} & a_{1,2} \\ a_{2,2} & a_{1,2} & a_{0,2} & a_{1,2} & a_{2,2} \end{bmatrix}.$$

These symmetries are necessary to make the mask operator a valid finite difference approximation to the Laplacian.

The result of the application of the mask a to an array u^k of values is described as the convolution of a and u^k

$$(a * u^k)_{i,j} = \sum_{m=-r}^{r} \sum_{n=-r}^{r} a_{m,n}\ u^k_{i+m,j+n}. \tag{4}$$

Think of $u^k_{i,j}$ as being obtained from a continuous function $u(t,x,y)$ evaluated at $t = t_k = k\,\Delta t$, $x = x_i = h\,i$, $y = y_j = h\,j$. Expand $u(t,x,y)$ in a Taylor series and use the symmetry properties (3) of the mask to obtain

$$\begin{aligned} (a * u^k)_{i,j} = \sum_{m=0}^{r} \sum_{n=1}^{r} \Big[& 4\,u(t_k,x_i,y_j) + \left(m^2+n^2\right)\left(u^{(0,0,2)}(t_k,x_i,y_j) + u^{(0,2,0)}(t_k,x_i,y_j)\right) h^2 \\ & + \frac{h^4}{12}\big((m^4+n^4)u^{(0,0,4)}(t_k,x_i,y_j) + 12m^2n^2u^{(0,2,2)}(t_k,x_i,y_j) \\ & \qquad + (m^4+n^4)u^{(0,4,0)}(t_k,x_i,y_j)\big) \\ & + \mathcal{O}(h^6)\Big] a_{m,n} + a_{0,0}\,u(t_k,x_i,y_j). \end{aligned} \tag{5}$$

Therefore the total effect of the mask a in terms of values u^k and $\nabla^2 u^k$ is

$$a * u^k = S \cdot u^k + h^2 \mathcal{D} \nabla^2 u^k + \frac{h^4}{12} E(u^k) + \mathcal{O}(h^6). \tag{6}$$

Then we assess the reliability of certain classes of masks by investigating their properties with regard to the propagation of wave fronts in excitable media. According to singular perturbation theory of traveling waves in two-dimensional excitable media [10,23,28,29], the normal velocity (N) of a wave front should be linearly related to its curvature (K): $N = c - D\,K$, where c is the velocity of a planar wave and D is the diffusion coefficient of the excitation variable. We show that only some classes of masks give a linear speed-curvature relation with slope D *independent* of the threshold for activation. Of these "good" masks, one class is especially noteworthy because it is computationally efficient.

2. Finite difference approximations to the Laplacian

The standard finite difference approximation to the Laplacian in two dimensions is the 5-point-cross

$$cross := \begin{bmatrix} 0 & 1 & 0 \\ 1 & -4 & 1 \\ 0 & 1 & 0 \end{bmatrix}.$$

Using this operator, the diffusion equation for $u(t, x, y)$,

$$\frac{\partial u}{\partial t} = D\ \nabla^2\ u, \tag{1}$$

can be solved using the finite difference scheme

$$u^{k+1} = u^k + \frac{\Delta t}{h^2} D \cdot cross * u^k, \tag{2}$$

where $\Delta t > 0$, $h > 0$, $u^k_{i,j}$ is the computed approximation to the solution $u(k\,\Delta t, ih, jh)$, and $*$ denotes the convolution operation $(cross * u^k)_{i,j} = u^k_{i,j+1} + u^k_{i,j-1} + u^k_{i+1,j} + u^k_{i-1,j} - 4\ u^k_{i,j}$. (Here and from now on u^k is a 2-dimensional array at time $k\Delta t$, which consists of elements $u^k_{i,j}$.) There is no reason why other masks might not be used instead of the 5-point-cross. In the following the implications of using different masks are investigated.

location within its unit cell. In this way they obtain a semi-random grid that covers the spatial domain in a rather uniform fashion, without the "clumps" and "bald spots" characteristic of a truly random distribution. Then they define the neighbors of cell i as all those grid points that lie within a circle of radius R centered on i. They sum up the total number of excited neighbors of a resting or recovering cell, and, if this sum exceeds a threshold, the central cell becomes excited. As for the uniform square neighborhoods of Gerhardt, Schuster, and Tyson, so here wave speed becomes linearly dependent on wave front curvature, but the circularity and slight nonuniformity of the Markus-Hess neighborhoods make wave speed nearly independent of direction relative to the underlying rectangular lattice. However, one must pay a steep price for isotropic wave propagation. Total excitation sums in the square neighborhoods of Gerhardt, Schuster, and Tyson can be computed by only four additions per grid point *independent of the "radius" r of the neighborhood,* but the sums for the random-circle neighborhoods of Markus and Hess require approximately πR^2 table lookups and πR^2 additions per grid point. The computational inefficiency of this method cancels the most important advantage of the CA approach.

Fast and Efimov [3] take a third approach. They point out correctly that the effect of an excited cell at a distance z from a resting cell should drop off with z. Thus, when calculating the sum-of-excitation in the neighborhood of a resting cell, the contribution from an excited cell at distance z should be weighted by a factor $w(z)$. Reasonable would be the choice

$$w(z) = \left\lfloor C\ e^{\frac{-z^2}{4d}} \right\rfloor ,$$

where $\lfloor \zeta \rfloor$ denotes the largest integer $\leq \zeta$; $\quad z^2 = (x - x_0)^2 + (y - y_0)^2$, (x_0, y_0) = location of central cell; and C and d determine the range of interaction ($R = \lfloor \sqrt{4d \log C} \rfloor$). Although such "Gaussian" masks give good results, as we shall show, they are also computationally inefficient, demanding a large number of additions and multiplications per grid point.

In this paper we present a general theory of "masks" as discrete approximations to the diffusion equation. We show how to calculate the effective diffusion coefficient of a mask from its weights.

recent theory of spatiotemporal organization in excitable media [8,9,16,17,18,23,25,30,31]. This hegemony of PDEs has come about because the original CA models lacked several essential features of excitable media [4,26]:

- Curvature. In two- and three-dimensional media, curved waves travel at speeds different from planar waves: concave waves travel slower, convex waves travel faster [10,28,29].
- Dispersion. The speed of a planar wave front depends on the extent of recovery of the medium immediately in front of the wave [2,14].
- Isotropy. In a homogeneous isotropic excitable medium, the speed of planar wave propagation should be the same in all directions, but early CA models exhibited gross anisotropies in wave speed relative to the underlying grid.

Many of these problems are rooted in the fact that classical CA models propagate waves at a single speed of one cell per time step (in the direction of the grid). To overcome this problem, it is necessary to introduce larger neighborhoods over which diffusion of excitation can operate in one time step. Several different groups have independently proposed CA models with expanded neighborhoods [3,4,5,6,12,13].

For instance, Gerhardt, Schuster, and Tyson [4,5,6] sum up all the excited cells within a square neighborhood of area $(2r+1)^2$, $r =$ integer $(1, 2, \cdots, 6)$. If this sum exceeds a certain threshold, then the central cell becomes excited in the next time step. They show that many effects of curvature are introduced merely by such an increase in the size of the neighborhood over which excitation can propagate in one time step. Furthermore, by making the threshold a function of the extent of recovery of the central cell, they incorporate dispersive effects into the CA rules. Though curvature effects ameliorate the anisotropy of wave propagation in this CA, they do not completely eliminate it.

Markus and Hess [12,13] show that anisotropy can be almost completely eliminated by somewhat randomizing the grid of cells. Like most other investigators, they adopt a rectangular lattice, but instead of placing each grid point at the center of a unit cell, they assign each grid point to a random

DIFFUSION AND WAVE PROPAGATION IN CELLULAR AUTOMATON MODELS OF EXCITABLE MEDIA*

Jörg R. Weimar †

John J. Tyson ‡

Layne T. Watson†

Abstract (1) We examine general "masks" as discrete approximations to the diffusion equation, showing how to calculate the diffusion coefficient from the elements of the mask. (2) We combine the mask with a thresholding operation to simulate the propagation of waves in excitable media, showing that (for well-chosen masks) the waves obey a linear "speed-curvature" relation with slope given by the predicted diffusion coefficient. (3) We assess the utility of different masks in terms of computational efficiency and adherence to a linear speed-curvature relation.

1. Introduction

Excitable media support undamped traveling waves of excitation, such as waves of membrane depolarization in nerve axons [7], waves of excitation in chemical reaction systems [25,27], and waves of star formation in galactic dust clouds [20]. In physical and chemical systems these waves provide striking examples of spontaneous symmetry breaking and spatiotemporal organization, and in biological systems they serve essential roles in cellular communication and organization. Although some of the first models of excitable media were based on the discrete cellular automaton (CA) approach [1,11,15,21,22,24], continuous partial differential equation (PDE) models have dominated

* This work was supported in part by National Science Foundation Grant DMS-8810456 and Department of Energy Grant DE-FG05-88ER25068.

† Department of Computer Science, Virginia Polytechnic Institute and State University, Blacksburg, Virginia 24061-0106, e-mail: weimar@cayuga.cs.vt.edu

‡ To whom correspondence should be addressed: Department of Biology, Virginia Polytechnic Institute and State University, Blacksburg, Virginia 24061-0406, e-mail: tyson@vtvm1.cc.vt.edu